IVYSPRING INTERNATIONAL PUBLISHER

Theranostics

2017; 7(2): 413-424. doi: 10.7150/thno.15712

Research Paper

Noninvasive Imaging of Myocardial Inflammation in Myocarditis using ^{68}Ga-tagged Mannosylated Human Serum Albumin Positron Emission Tomography

Seung-Pyo Lee[1,2*], Hyung-Jun Im[3*], Shinae Kang[4], Seock-Jin Chung[3], Ye Seul Cho[1], Hyejeong Kang[1], Ho Seon Park[4], Do-Won Hwang[3], Jun-Bean Park[1,2], Jin-Chul Paeng[3], Gi-Jeong Cheon[3], Yun-Sang Lee[3], Jae Min Jeong[3#✉], Yong-Jin Kim[1,2#✉]

1. Cardiovascular Center, Seoul National University Hospital;
2. Department of Internal Medicine, Seoul National University College of Medicine;
3. Department of Nuclear Medicine, Seoul National University Hospital and Seoul National University College of Medicine;
4. Department of Internal Medicine, Gangnam Severance Hospital, Yonsei University College of Medicine, Seoul, South Korea.

*These authors contributed equally as first authors.

#These authors contributed equally as corresponding authors.

✉ Corresponding author: Jae Min Jeong, PhD. Department of Nuclear Medicine, Seoul National University Hospital and Seoul National University College of Medicine, Daehak-ro 101, Jongno-gu, Seoul, South Korea, 03080. E-mail: jmjng@snu.ac.kr AND Yong-Jin Kim, MD, PhD. Cardiovascular Center, Seoul National University Hospital and Department of Internal Medicine, Seoul National University College of Medicine, Daehak-ro 101, Jongno-gu, Seoul, South Korea, 03080. Tel: 82-2-2072-1963 FAX: 82-2-2072-2577 E-mail: kimdamas@snu.ac.kr.

Received: 2016.04.01; Accepted: 2016.10.27; Published: 2017.01.01

Abstract

The diagnosis of myocarditis traditionally relies on invasive endomyocardial biopsy but none of the imaging studies so far are specific for infiltration of the inflammatory cells itself. We synthesized ^{68}Ga-2-(p-isothiocyanatobenzyl)-1,4,7-triazacyclononane-1,4,7-triacetic acid (NOTA) mannosylated human serum albumin (MSA) by conjugating human serum albumin with mannose, followed by conjugation with NOTA and labeling it with ^{68}Ga. The efficacy of ^{68}Ga-NOTA-MSA positron emission tomography (PET) for imaging myocardial inflammation was tested in a rat myocarditis model. A significant number of mannose receptor-positive inflammatory cells infiltrated the myocardium in both human and rat myocarditis tissue. ^{68}Ga-NOTA-MSA uptake was upregulated in organs of macrophage accumulation, such as liver, spleen, bone marrow and myocardium (0.32 (0.31~0.33) for normal versus 1.02 (0.86~1.06) for myocarditis (median (range), SUV); n=4~6 per group, p-value=0.01). ^{68}Ga-NOTA-MSA uptake in the left ventricle was upregulated in myocarditis compared with normal rats (2.29 (1.42~3.40) for normal versus 4.18 (3.43~6.15) for myocarditis (median (range), average standard uptake value ratio against paraspinal muscle); n=6 per group, p-value<0.01), which was downregulated in rats with cyclosporine-A treated myocarditis (3.69 (2.59~3.86) for myocarditis versus 2.28 (1.76~2.60) for cyclosporine-A treated myocarditis; n=6 per group, p-value<0.01). The specificity of the tracer was verified by administration of excess non-labeled MSA. ^{68}Ga-NOTA-MSA uptake was significantly enhanced earlier in the evolution of myocarditis before any signs of inflammation could be seen on echocardiography. These results demonstrate the potential utility of visualizing infiltration of mannose receptor-positive macrophages with ^{68}Ga-NOTA-MSA PET in the early diagnosis of as well as in the monitoring of treatment response of myocarditis.

Key words: myocarditis, macrophage, mannose receptor, positron emission tomography, molecular imaging.

Introduction

Myocarditis is a condition defined as a pathological immune response in the myocardium by noxious stimuli and is characterized by massive infiltration of immune cells, especially macrophages (1). Clinically, myocarditis can lead to sudden death or acute heart failure and in the long term, chronic

dilated cardiomyopathy (2). Therefore, the proper diagnosis is important in patients with suspected myocarditis.

The traditional gold standard method of diagnosing myocarditis has been to prove the active inflammation of the myocardium with endomyocardial biopsy (3), supported by biochemical evidence of active myocardial damage (4), and by visualizing indirect evidence of myocardial inflammation, such as myocardial edema on various imaging studies (5). However, none of these are specific for imaging myocardial inflammation nor the infiltration of the inflammatory cells itself.

Molecular imaging may be useful for visualizing active myocardial inflammation or infiltration of inflammatory cells. Specifically, macrophages are major effector cells in myocarditis (1) and development of macrophage-specific tracers may aid in the diagnosis of myocarditis, the follow-up of the inflammatory status noninvasively and furthermore, development of new treatment strategies (6). In this work, we hypothesized that it would be possible to image myocardial inflammation using a novel positron-emitting agent, ^{68}Ga-2-(p-isothiocyanato-benzyl)-1,4,7-triazacyclononane-1,4,7-triacetic acid (NOTA) mannosylated human serum albumin (MSA), that we initially described as a lymph node imaging agent (7).

Materials and Methods

Synthesis of ^{68}Ga-NOTA-MSA

A detailed description of the synthesis process and the labeling efficiencies, radiochemical purities have been published elsewhere (7). NOTA-MSA was synthesized following two steps; 1) Conjugation of α-D-mannopyranosylphenyl isothiocyanate to human serum albumin (HSA), resulting in MSA. 2) Conjugation of MSA from the first step with (p-SCN-Bn)-NOTA, resulting in NOTA-MSA. MSA was synthesized by conjugating 20mg HSA (Sigma-Aldrich, St. Louis, MO, USA) with 5.5mg SCN-mannose (Sigma-Aldrich) in 0.1M sodium carbonate buffer (pH 9.5) for 20 hours. The MSA was again conjugated with 10mg 2-(p-isothiocyanato-benzyl)-1,4,7-triazacyclononane-1,4,7-triacetic acid (SCN-NOTA) in the same buffer for 2 hours. 1mg NOTA-MSA in 1mL normal saline was mixed with 1mL $^{68}GaCl_3$ (in 0.1N HCl) (^{68}Ge/^{68}Ga generator from Eckert & Ziegler, Berlin, Germany) to generate the final product, ^{68}Ga-NOTA-MSA.

Animal models of myocarditis

Protocols of animal studies were approved by the institutional animal care and use committee and experiments using the radioactive tracers were approved by the institutional biosafety committee of Seoul National University Hospital. Quantitations of echocardiography and positron emission tomography (PET) images were done in a blinded manner.

A mixture of 1mg (10mg/mL) porcine cardiac myosin (Sigma-Aldrich, St. Louis, MO, USA) with an equal volume of complete Freund's adjuvant (Sigma-Aldrich) was injected into the footpad subcutaneously at days 1 and 8 in 7-week old male Lewis rats (Orient Bio, Seongnam-si, Gyeonggi-do, Korea) (8,9). Cyclosporine-A (Sigma-Aldrich) was given intraperitoneally daily (5mg/kg) starting from the indicated day for treatment of myocarditis. Transthoracic echocardiography (Nemio, Toshiba Co., Tokyo, Japan) was performed weekly starting from day 1. The animals were anesthetized using the lowest dose of isoflurane (4% initially and then 2~3% for maintenance) as possible with mixed oxygen. The left ventricular (LV) wall thickness at end-diastole, LV end-diastolic/systolic dimensions (LVEDD/LVESD) was measured at the papillary muscle level using the M-mode echocardiography. The LV fractional shortening was calculated as (LVEDD-LVESD)/ LVEDD. Animals were sacrificed at day 22 after taking the ^{68}Ga-NOTA-MSA PET. The ^{68}Ga-NOTA-MSA uptake in each organ was measured by the radioactivity of each organ using an automated γ-counter (Cobra II, Packard Instruments, Meriden, CT) 1 hour post-injection and the results expressed as standard uptake value (SUV). SUV was calculated as (decay-corrected activity/unit tissue weight)/ (injected activity/body weight).

PET/CT imaging and analysis

The ^{68}Ga-NOTA-MSA radioactive tracer (55.5 MBq) was injected via tail vein and dynamic images were acquired for 60 minutes' post-injection with a dedicated PET/CT scanner (eXplore VISTA, GE Healthcare, WI, USA). After confirming that the distribution of ^{68}Ga-NOTA-MSA reached pseudoequilibrium 40 minutes' post-injection (Figure 1), a 20 minute static image was acquired at 40~60 minutes post-injection. The PET scans were performed and reconstructed as previously described (10). In brief, the scan images were reconstructed using a 3-dimensional ordered-subsets expectation maximum algorithm with random and scatter corrections. Attenuation correction was done using corresponding CT scan. The voxel size was 0.3875×0.3875×0.775 mm. For autoradiography, the heart was sectioned into 20μm thick short-axis slices and exposed to a radiosensitive image plate (11). FLA 2000 system (Fuji, Tokyo, Japan) was used for the autoradiography experiment.

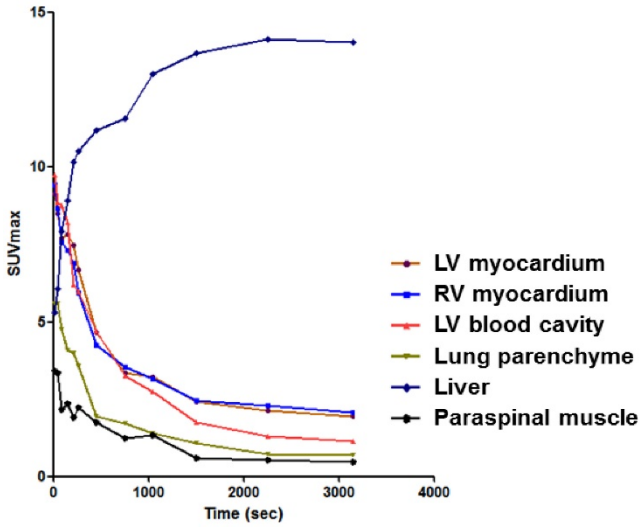

Figure 1. Distribution pattern of ^{68}Ga-NOTA-MSA according to time in various organs or tissues. LV, left ventricle; RV, right ventricle; SUV, standard uptake value.

The region of interest (ROI) templates were used for measuring uptake of LV and RV. The ROI templates were made using ^{11}C-peripheral benzodiazepine receptor (PBR) images of the normal rat heart. The PBR, also known as translocator protein, is an avid protein that is highly expressed in the myocardium (12,13). We could clearly delineate LV and RV using the PET images of ^{11}C-PBR, which is an established translocator protein imaging agent. Isocontour function using a threshold of 40% of maximal uptake was used to make template ROIs for LV and RV. The size and axis of the template ROIs were adjusted according to the outer contour of each rat's heart based on its CT images. As there was a substantial spillover of the signal from the liver, we cautiously excluded the lower part of the LV or RV ROI that is overlaid by the liver uptake. The 0.1cm^3-sized spherical ROI was also drawn on the left paraspinal muscle at the level of upper T-spines to quantify the background tracer uptake. Average/maximal standardized uptake value (SUV) was defined as average/maximal SUV of total voxels in the ROIs. Maximal myocardium to paraspinal muscle SUV ratio (maximal SUVR) was defined as maximal SUV of the myocardium divided by maximal SUV of the paraspinal muscle. Average myocardium to paraspinal muscle SUV ratio (average SUVR) was defined as average SUV of the myocardium divided by average SUV of the paraspinal muscle. In experiments using unlabeled MSA for blockade of ^{68}Ga-NOTA-MSA binding in vivo, a 150-fold excess of unlabeled MSA was administered intravenously 10 minutes prior to tracer injection. All image analysis and visualization were done using PMOD software (PMOD Technologies Ltd, Zurich, Switzerland).

For the comparison of ^{68}Ga-NOTA-MSA PET with ^{18}F-fluorodeoxyglucose (^{18}F-FDG) PET for imaging myocarditis, all rats were kept fasting for >15 hours and the ^{18}F-FDG (37 MBq) injected intraperitoneally. The images were acquired after 1 hour of injecting the ^{18}F-FDG. The analysis method was identical to that of the ^{68}Ga-NOTA-MSA PET images.

Flow cytometry of MSA uptake

RAW 264.7 cells (ATCC, Manassas, VA) were cultured (DMEM supplemented with 5% fetal bovine serum) and the cells were incubated with 0.01mg/mL rhodamine isothiocyanate (RITC)-tagged HSA, RITC-MSA or ^{68}Ga-NOTA-MSA for 1 hour. The signal intensity, count of the cells was analyzed using the flow cytometry machine (BD FACSCalibur™, BD Biosciences, San Jose, CA) and program (BD FACSDiva™, BD Biosciences) or an automated gamma counter (Cobra II 5003, Packard Bioscience, Meridien, CT). MSA binding was blocked with the indicated concentration of unlabeled MSA, 1 hour before incubation with RITC-MSA or ^{68}Ga-NOTA-MSA.

Human studies

Biopsy samples were obtained from 4 patients diagnosed with myocarditis and from 3 patients who underwent a routine endomyocardial biopsy after heart transplantation. The 3 heart transplantation patients did not have any symptoms or signs of rejection. The study was conducted in accordance with the latest Declaration of Helsinki and the institutional review board approved the study protocol.

Immunohistochemical, immunofluorescent staining

Myocardial specimens were fixed and the midventricular section was made into paraffin blocks. Primary antibodies used for immunohistochemistry were anti-ED-1 (EMD Millipore, Billerica, MA) for macrophages and anti-mannose receptor (MR) (Abcam, Cambridge, MA) for mannose receptor. These were incubated with appropriate secondary antibodies and visualized using the DAB substrate kit or secondary antibodies conjugated with the appropriate immunofluorescence reporter. For visualization of MSA uptake, RITC-MSA was given during the secondary antibody incubation step in the tissue section. All images were taken with either a slide scanner (Leica SCN400, Leica microsystems, Wetzlar, Germany) for the immunohistochemical specimens or a confocal microscopy (LSM 710, Carl Zeiss, Jena, Germany) for the immunofluorescent staining.

Statistical analyses

All data are presented as median (together with the range where needed) and analyzed using the Mann-Whitney U-test. The degree of trend was tested using the extended Mantel-Haenszel Chi-square for linear trend. Graphs were drawn with GraphPad Prism 7.0 (GraphPad Software Inc., San Diego, CA). A two-tailed p-value<0.05 was considered statistically significant and all statistical analysis was done using the SPSS version 21.0 software (SPSS, Chicago, IL).

Results

Infiltration of MR-positive macrophages in myocarditis and the uptake of ^{68}Ga-NOTA-MSA by macrophages

Human endomyocardial biopsy samples of myocarditis demonstrated extensive myocardial destruction with interstitial infiltration of inflammatory cells (Figure 2A). Immunohisto-chemical MR staining demonstrated that a significant majority of these cells were MR-positive (Figure 2B). There were minimal inflammatory or MR-positive cells in the myocardial specimens taken from normal heart transplantation recipients.

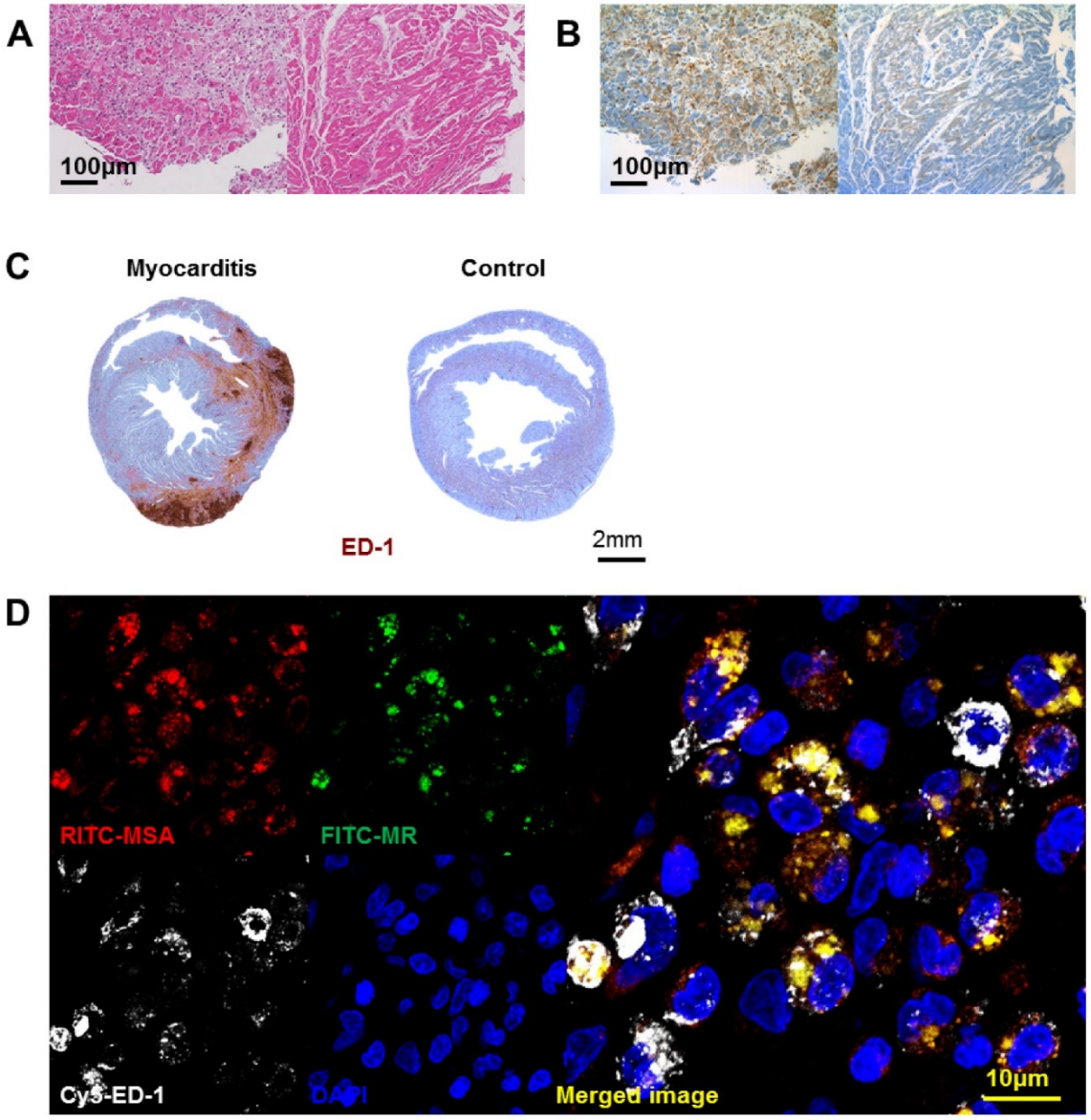

Figure 2. Infiltration of mannose receptor-positive macrophages in myocarditis. (A) Inflammatory cells infiltrated the myocardium significantly in human myocarditis sample (left panel) as compared to normal human myocardium in heart transplantation recipients (right panel). H&E staining. (B) Adjacent section of samples in Figure 2A identified a significant proportion of the inflammatory cells to be positive for mannose receptor (brown color) in human myocarditis (left panel) as compared to normal human myocardium (right panel). Representative mannose receptor immunostaining images. n=3~4 per group. (C) Inflammatory cells significantly infiltrated the myocardium in the rat myocarditis sample (left panel) as compared to minimal in the normal rat myocardium (right panel). Representative ED-1 immunostaining images. (D) RITC-MSA binds to mannose receptor-positive cells in rat myocarditis, which in turn are ED-1 positive. Red, MSA; green, mannose receptor (MR); white, ED-1; blue, DAPI.

We harvested the rat heart after 3 weeks of porcine cardiac myosin injection, the timepoint of maximal inflammation as in a previous report (8). Extensive ED-1-positive inflammatory cell infiltration was noted in the myocardium of the myocarditis rats (Figure 2C). The MSA distribution pattern colocalized to the areas positive for MR, suggesting that MSA uptake is associated with MR (Figure 2D). The cells positive for MR and for MSA binding ex vivo were positive for ED-1, suggesting that macrophages are the major cells responsible for MSA uptake.

In vivo biodistribution of ^{68}Ga-NOTA-MSA in rats under myocarditis

We analyzed the pattern of ^{68}Ga-NOTA-MSA distribution in control and myocarditis rats, 1 hour post-injection of the tracer after 3 weeks of inflammation. The biodistribution assay demonstrated significantly higher tracer uptake in the spleen, kidney and the heart in the myocarditis than the normal rats (Table 1). There was a 3.2-fold higher γ-emission from the myocardium of the myocarditis compared with that of the control rats (Figure 3), the degree of which was higher than any other organ.

Table 1. Postmortem biodistribution of ^{68}Ga-NOTA-MSA of each organ in normal control rats versus the myocarditis rats.

	Normal (n=4, SUV)	Myocarditis (n=6, SUV)	p-value
Blood	0.74 (0.74~0.76)	0.67 (0.19~0.82)	0.114
Paraspinal muscle	0.05 (0.04~0.06)	0.05 (0.04~0.07)	0.746
Lung	1.34 (1.13~1.57)	1.01 (1.00~1.75)	0.257
Liver	19.64 (16.60~20.34)	19.82 (17.28~21.65)	0.762
Spleen	8.72 (7.32~9.19)	12.20 (10.46~13.23)	0.010
Intestine	0.06 (0.04~0.27)	0.15 (0.07~0.33)	0.114
Kidney	0.72 (0.70~0.76)	0.87 (0.80~1.00)	0.010
Bone marrow	2.04 (1.79~2.15)	2.17 (1.86~2.72)	0.352
Heart	0.32 (0.31~0.33)	1.02 (0.86~1.06)	0.010

All values presented as median (range). SUV, standard uptake value.

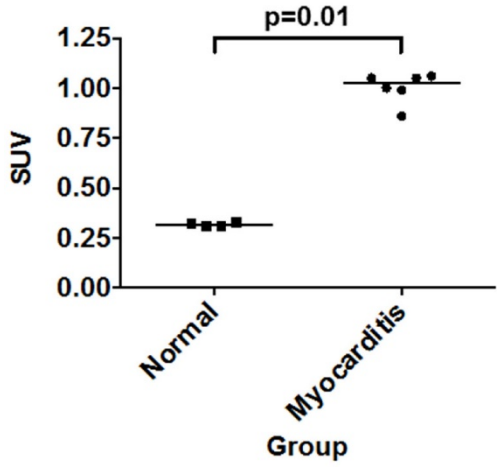

Figure 3. Uptake of ^{68}Ga-NOTA-MSA in the myocardium. Post-mortem biodistribution of ^{68}Ga-NOTA-MSA in the myocardium of normal versus myocarditis rats, 1 hour post-injection of the tracer. Median values of each groups are shown as horizontal lines. SUV, standard uptake value.

^{68}Ga-NOTA-MSA for the diagnosis of myocardial inflammation in myocarditis

Compared with the normal rats (Figure 4A and Supplementary Movie S1), the ^{68}Ga-NOTA-MSA uptake in the myocardium was significantly higher in the myocarditis rats (Figure 4B and Supplementary Movie S2). The localization of ED-1-positive inflammatory cells overlapped with the ^{68}Ga-NOTA-MSA autoradiography (Figure 4C). Although the systolic function was not significantly different (Supplementary Figure S1A), the LV myocardium was significantly thicker in the myocarditis rats (Figure 4D). The average SUVR in both ventricles was significantly higher in the myocarditis rats (Figure 4E and 4F), as well as the maximal SUVR (Supplementary Figure S1B and S1C). There was no overlap in the degree of ^{68}Ga-NOTA-MSA uptake between the myocarditis versus the normal rats.

Specificity of ^{68}Ga-NOTA-MSA uptake for inflammatory cell imaging

After confirming the colocalization of MSA binding and MR expression in the myocardium by tissue staining (Figure 2D), we further investigated the specificity of the tracer. A strong fluorescent signal shift was found in RITC-MSA treated RAW 264.7 cells, indicating substantial tracer uptake by the cells, while a minimal shift was shown in non-mannosylated RITC-HSA treated cells (Figure 5A). Furthermore, pretreatment with excess unlabeled MSA attenuated the signal in a dose-dependent manner (Figure 5B and 5C), confirming the specific uptake of RITC-MSA by a macrophage cell line. Also, similar findings were observed when ^{68}Ga-NOTA-MSA was used instead of RITC-MSA (data not shown).

Interestingly, after administration of unlabeled MSA in the myocarditis rats, the uptake of ^{68}Ga-NOTA-MSA in the liver and the spleen, the major reticuloendothelial organs that harbor the inflammatory cells, were significantly attenuated to half or one-third. This was associated with significant increase of ^{68}Ga-NOTA-MSA uptake in other organs, including the myocardium and the blood pool (Figure 5D). However, the pattern of myocardial uptake in the myocarditis rats pretreated with unlabeled MSA was different from that in the myocarditis rats. Whereas the ^{68}Ga-NOTA-MSA uptake was focally increased and associated with the sites of macrophage infiltration in the myocarditis rats, the uptake was diffusely enhanced and was not associated with the site of the macrophage infiltration in the myocarditis rats pretreated with unlabeled MSA (Figure 5E).

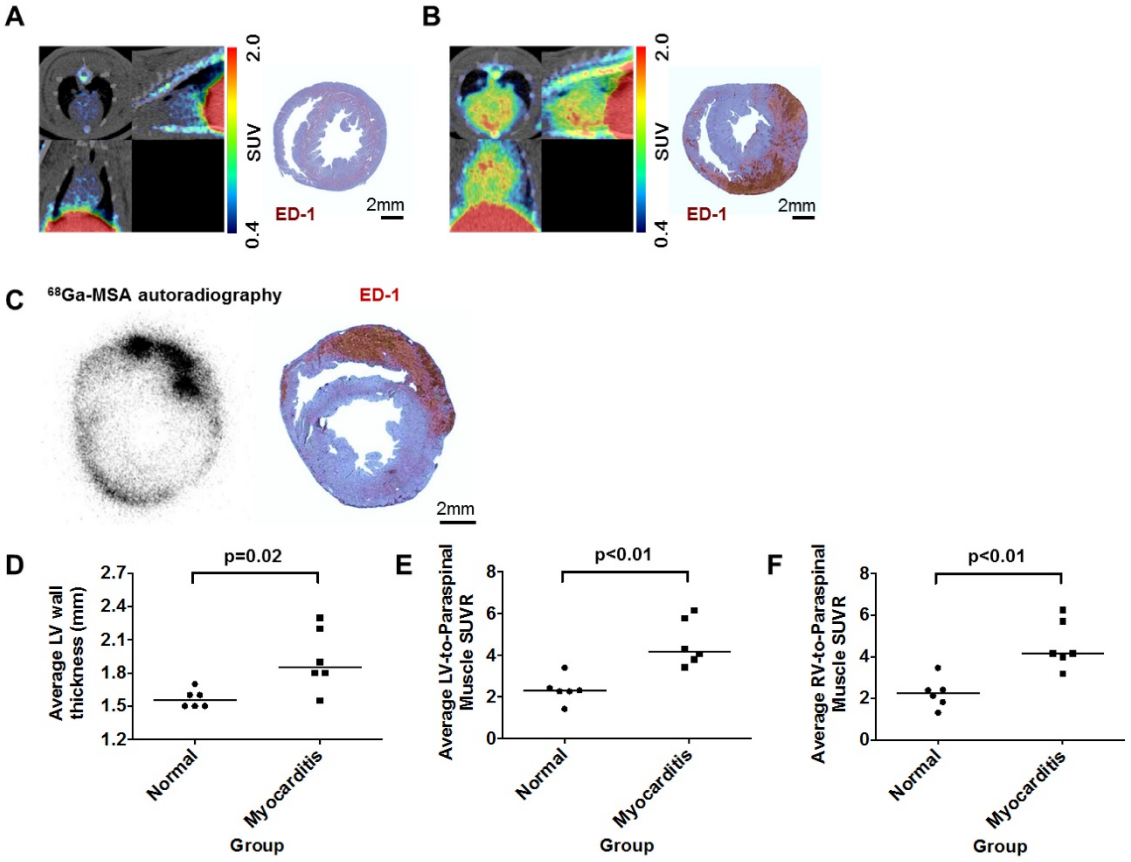

Figure 4. ^{68}Ga-NOTA-MSA PET imaging for the diagnosis of myocardial inflammation in myocarditis rats. (A and B) Representative ^{68}Ga-NOTA-MSA images and the corresponding ED-1 staining results for inflammatory cells (brown color) in normal (A) versus myocarditis (B) rats. Higher ^{68}Ga-NOTA-MSA was noted in the myocarditis rats compared with the normal rats, which was corroborated by the massive infiltration of inflammatory cells in the immunohistochemistry. (C) The ^{68}Ga-NOTA-MSA uptake pattern in the myocardium by autoradiography colocalizes with the pattern of inflammatory cell infiltration by ED-1 immunostaining (brown color) in rat myocarditis. (D) Significantly thicker left ventricle (LV) wall in the myocarditis rats compared with the normal rats by M-mode echocardiography. (E and F) Significantly higher average ^{68}Ga-NOTA-MSA uptake at the LV (E) and the right ventricle (RV) (F) in the myocarditis rats compared with the normal rats. The median value of each groups are shown as horizontal lines in (D), (E) and (F). SUV(R), standardized uptake value (ratio).

^{68}Ga-NOTA-MSA for monitoring the efficacy of myocarditis treatment

Rats with myocarditis were treated with systemic cyclosporine-A after the initial dose of porcine cardiac myosin immunization (14). In contrast to the inflammatory cell infiltration in rats with myocarditis, rats co-treated with cyclosporine-A did not show any sign of inflammation in the myocardium (Figure 6A and 6B). Although there was no difference in the LV systolic function between both groups (Supplementary Figure S2A), co-treatment with cyclosporine-A significantly decreased the average LV wall thickness (Figure 6C). Average SUVR in both ventricles was significantly higher in the myocarditis rats compared with the cyclosporine-A co-treated rats (Figure 6D and 6E), as well as the maximal SUVR (Supplementary Figure S2B and S2C).

To fully dissect the potential clinical benefit of ^{68}Ga-NOTA-MSA PET in the image-based identification of inflammation, we also investigated whether there would be changes in the degree of ^{68}Ga-NOTA-MSA uptake according to the treatment duration of cyclosporine-A. There was a decrease in the degree of ^{68}Ga-NOTA-MSA uptake in the myocardium according to the treatment duration of cyclosporine-A (Figure 6F). This decreasing trend of ^{68}Ga-NOTA-MSA uptake was dependent on the duration of cyclosporine-A treatment (Figure 6G), suggesting that the ^{68}Ga-NOTA-MSA PET may indeed be used for monitoring the response to treatment.

Comparison of the efficacy of the ^{68}Ga-NOTA-MSA with ^{18}F-FDG for myocarditis imaging

As ^{18}F-FDG is widely used for imaging of inflammation (15), we compared the efficacy of ^{68}Ga-NOTA-MSA to visualize the degree of inflammation with ^{18}F-FDG in myocarditis. The PET/CT scans were taken from the identical set of rats using both ^{18}F-FDG and ^{68}Ga-NOTA-MSA. The hotspots of myocardial inflammation matched between the ^{18}F-FDG and ^{68}Ga-NOTA-MSA PET scans

in some animals (Figure 7A). However, despite the similar degree of inflammatory cell infiltration between the animals (Figure 7B), this was not accurately mirrored in the ^{18}F-FDG PET images (Figure 7C). This was in contrast to the similar degree of the radioactive tracer uptake in the ^{68}Ga-NOTA-MSA PET scans (Figure 7D). Additionally, the extended fasting protocol was needed to suppress the normal uptake of glucose in the normal myocardium as suboptimal fasting of animals <8 hours resulted in nonspecific uptake of ^{18}F-FDG in the whole myocardium (data not shown). Taken together, the efficacy of ^{68}Ga-NOTA-MSA PET was at least as effective as or even better than ^{18}F-FDG PET.

^{68}Ga-NOTA-MSA for early detection of myocardial inflammation before structural changes in the myocardium

Additionally, we tested whether ^{68}Ga-NOTA-MSA PET could be used for detection of myocardial inflammation before overt changes in the myocardium ensues, for example, myocardial edema. Clinically, it is difficult to demonstrate whether there is any myocardial inflammation by conventional imaging studies and demonstration of myocardial inflammation would be highly desirable for early diagnosis.

All rats were followed with echocardiography and ^{68}Ga-NOTA-MSA PET weekly. Although there were no signs of myocardial inflammation 2 weeks post-immunization of the initial dose of porcine cardiac myosin, a group of rats showed myocardial edema and pericardial effusion on echocardiography by 3 weeks post-immunization (Figure 8A). The average systolic function of the rats was not significantly different throughout the study. However, the rats demonstrated an increase of ^{68}Ga-NOTA-MSA uptake as early as 2 weeks post-immunization compared with the baseline images and the uptake was maintained at 3 weeks (Figure 8B). The ^{68}Ga-NOTA-MSA uptake by week 2 was significantly higher than the baseline level in all animals tested (Figure 8C).

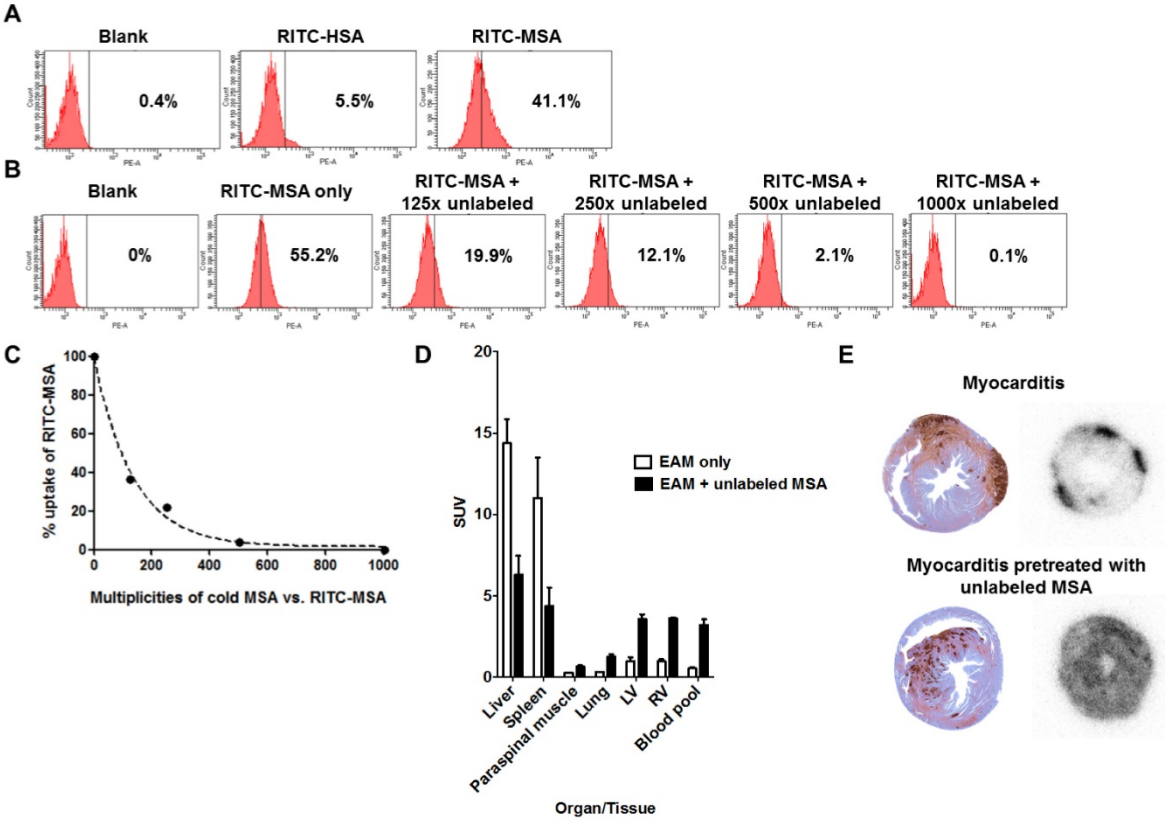

Figure 5. Specificity of ^{68}Ga-NOTA-MSA uptake in myocarditis. (A) Mannosylation is needed for uptake of the tracer in RAW 264.7 cell line. (B and C) The degree of RITC-MSA uptake is decreased by pretreatment of cold, unlabeled MSA in a dose-dependent manner. (D) Compared with the myocarditis only rats, the ^{68}Ga radiotracer signals in myocarditis rats pretreated with unlabeled MSA is decreased in the liver and the spleen, whereas the signal is significantly increased in other organs/tissues including the myocardium and the blood cavity. n=3 per group. SUV, mean standardized uptake value. (E) Autoradiography of the rat hearts demonstrate focally increased ^{68}Ga-NOTA-MSA uptake in the myocarditis rats (upper right panel), whereas the signal was diffusely increased in general in the myocarditis rats pretreated with unlabeled MSA (lower right panel). However, the degree of myocardial inflammation is similar between the two representative rats (upper and lower left panels). EAM, experimental autoimmune myocarditis.

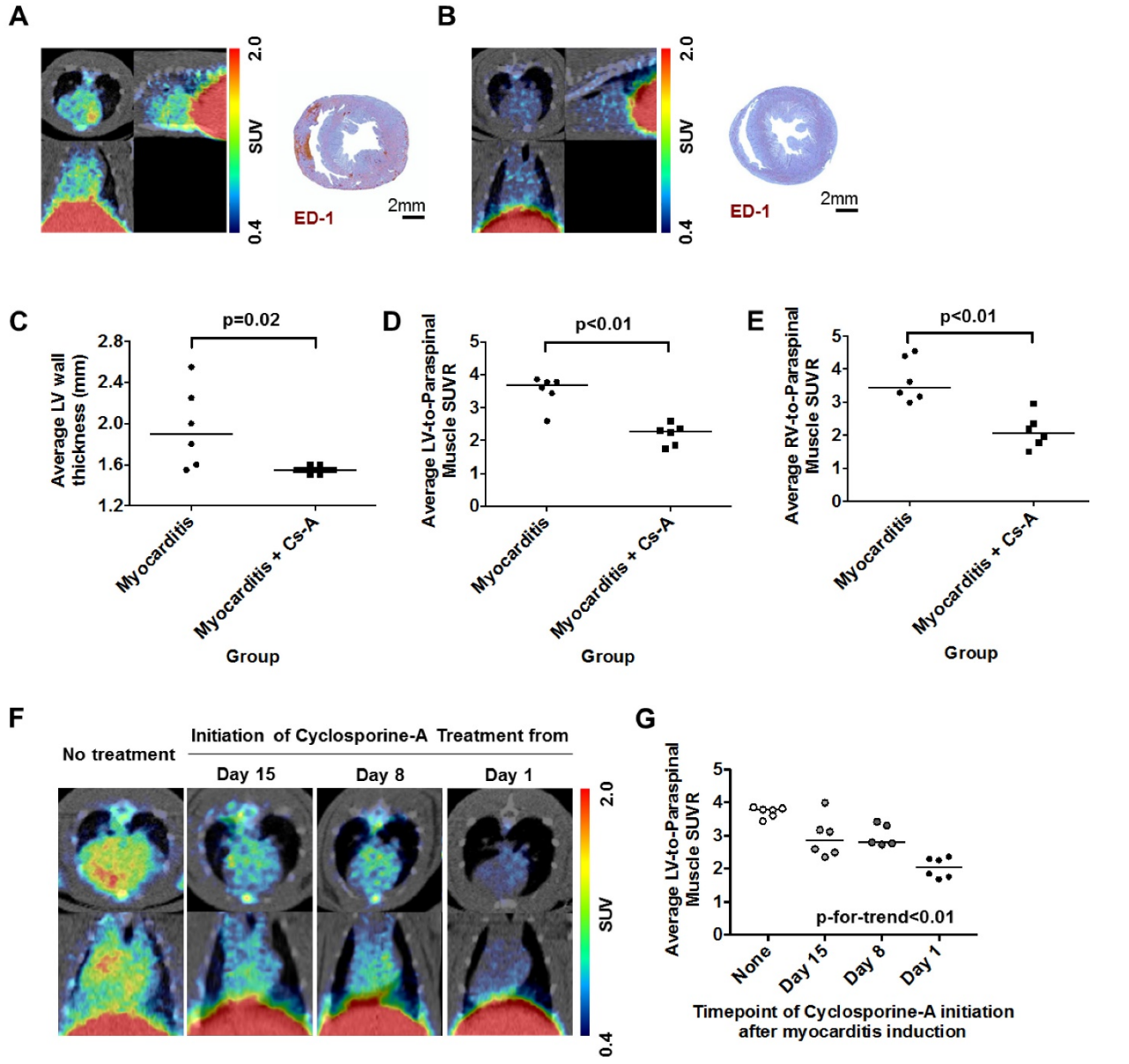

Figure 6. ^{68}Ga-NOTA-MSA PET imaging for the follow-up of treatment efficacy in myocarditis rats. (A and B) Representative ^{68}Ga-NOTA-MSA PET images and the corresponding ED-1 staining results for inflammatory cells (brown color) in the non-treated myocarditis rats (A) versus the myocarditis rats treated with cyclosporine-A (B). Higher ^{68}Ga-NOTA-MSA uptake was noted in the non-treated myocarditis rats compared with the myocarditis rats treated with cyclosporine-A, which was supported by the infiltration of inflammatory cells in the immunohistochemistry. (C) Significant regression of the left ventricle (LV) hypertrophy/edema was noted in the myocarditis rats treated with cyclosporine-A compared with the non-treated myocarditis rats by M-mode echocardiography. (D and E) Significantly lower average ^{68}Ga-NOTA-MSA uptake at the LV (D) and the right ventricle (RV) (E) in the myocarditis rats treated with cyclosporine-A compared with the non-treated myocarditis rats. The median value of each groups are shown as horizontal lines in (C), (D) and (E). (F) The uptake of ^{68}Ga-NOTA-MSA decreases with the duration of cyclosporine-A treatment. (G) A significant trend is noted in the decrease of ^{68}Ga-NOTA-MSA uptake with the increase in the duration of cyclosporine-A treatment. Cs-A, cyclosporine-A; SUV(R), standardized uptake value (ratio).

Discussion

In this study, we investigated the efficacy of a novel PET tracer, ^{68}Ga-NOTA-MSA, as a potential pharmaceutical for the diagnosis and monitoring of myocarditis. The novel findings are: 1) ^{68}Ga-NOTA-MSA uptake is associated with the MR of the macrophages. 2) This characteristic of ^{68}Ga-NOTA-MSA, together with the infiltration of MR-positive macrophages, enables noninvasive diagnosis of myocarditis. 3) ^{68}Ga-NOTA-MSA PET is effective for disease monitoring. 4) ^{68}Ga-NOTA-MSA PET is useful for early diagnosis of myocarditis before myocardial edema ensues. Collectively, ^{68}Ga-NOTA-MSA PET enables noninvasive diagnosis and monitoring of myocardial inflammation in myocarditis.

The MSA was initially developed for sentinel lymph node imaging as a single photon emission computed tomography agent by tagging the ^{99m}Tc (16,17) and revised recently for PET imaging agent (7). Mannose and human serum albumin are nontoxic, making it suitable for an optimal imaging agent. The

receptor of mannose residue is known to be expressed in M2 macrophages (18). A significant proportion of macrophages are positive for MR in rodent myocarditis models (1,19,20) and our staining results of human myocardial biopsy samples suggest that these cells may be significantly associated with the evolution of human myocarditis, thus providing a diagnostic basis of tracking MR-positive macrophages in myocarditis. Thinking of the potential benefit that albumin can be taken up by phagocytic cells and that ^{68}Ga-NOTA-MSA has 10~11 mannose residues in one albumin structure (7), we postulated that ^{68}Ga-NOTA-MSA would be an excellent molecule for imaging MR-positive macrophages.

The clear difference of ^{68}Ga-NOTA-MSA uptake between the normal and myocarditis rats demonstrate that PET imaging is useful for visualization of the degree of inflammation. Various imaging modalities such as echocardiography and cardiac magnetic resonance imaging are not specific for visualization of the cellular or molecular process. Previous investigators using PET have focused on ^{18}F-FDG for the diagnosis of myocarditis (21-23). However, not only have the reports remained as case reports, the utility of ^{18}F-FDG has not been supported by appropriate experimental studies. In our experiments, extensive fasting for >15 hours was needed to suppress the normal glucose uptake in the myocardium and the sensitivity of ^{18}F-FDG to detect the inflammatory cell infiltration seemed to be lower than that of ^{68}Ga-NOTA-MSA in some animals, questioning the sensitivity of ^{18}F-FDG PET for imaging myocardial inflammation. Sugar monomer-based imaging depends on the transporter (24), the function and expression of which may change according to the tissue status itself. In contrast, MR, upon engagement by ligands, is shuttled to the endocytotic vesicle (25). Other tracers, such as iron oxide nanoparticles (9), are nonspecifically phagocytosed by any immune cells (26). Although radiolabeled albumin itself may be a potential candidate for inflammation imaging, previously published reports by our group and others (27,28) have verified that the blood pool uptake of the radioactive tracer is substantial at several hours after injection. This can delay optimal imaging time point and hamper accurate measurement of myocardial tracer uptake. On the contrary, ^{68}Ga-NOTA-MSA showed rapid clearance from the blood pool which enabled us to image within 1 hour after the injection without the interference of blood pool uptake in our experiments (Figure 1). Therefore, the development of ^{68}Ga-NOTA-MSA PET for the diagnosis of myocarditis and the quantification of the degree of inflammation is potentially important for future clinical application and the mechanisms unique.

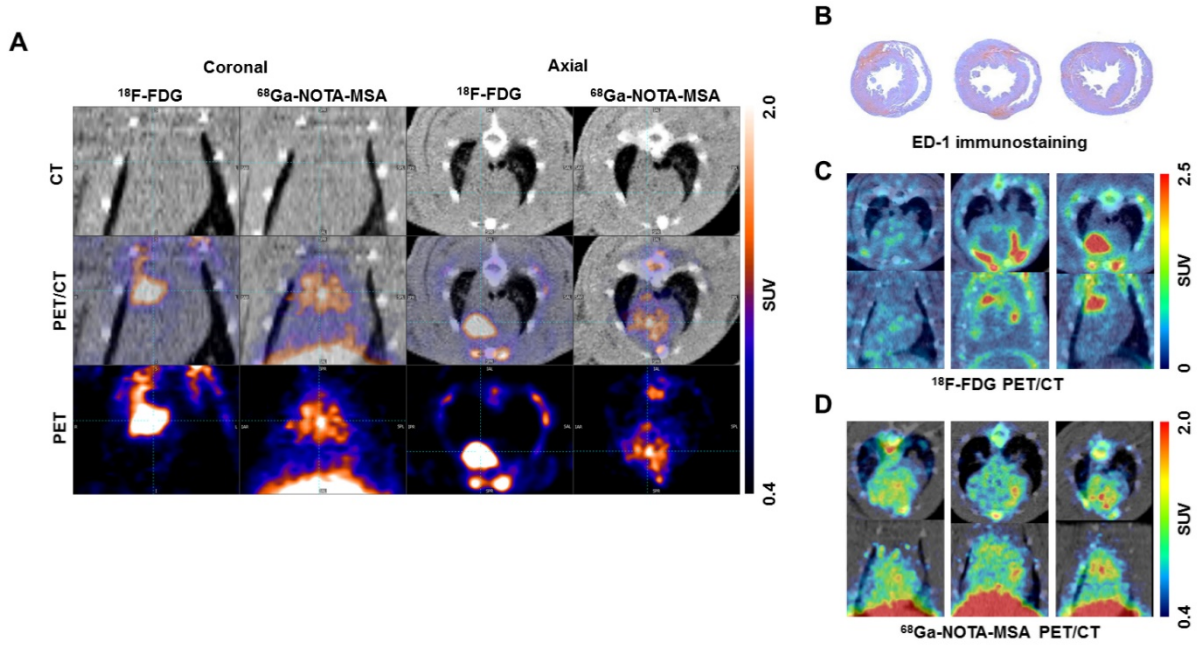

Figure 7. Comparison of ^{18}F-FDG and ^{68}Ga-NOTA-MSA PET for detection of myocardial inflammation in myocarditis. (A) The hotspots of myocardial inflammation colocalizes between the ^{18}F-FDG and ^{68}Ga-NOTA-MSA PET scans in some animals. (B~D) Different degree of ^{18}F-FDG and ^{68}Ga-NOTA-MSA uptake in spite of the similar degree of inflammatory cell infiltration. (B) Similar degree of inflammatory cell infiltration on ED-1 immunostaining. (C) Different degree of ^{18}F-FDG uptake between the animals, despite similar degree of inflammatory cell infiltration. (D) Similar degree of ^{68}Ga-NOTA-MSA uptake between the animals, matching the pathology findings on Figure 7B. SUV, standardized uptake value.

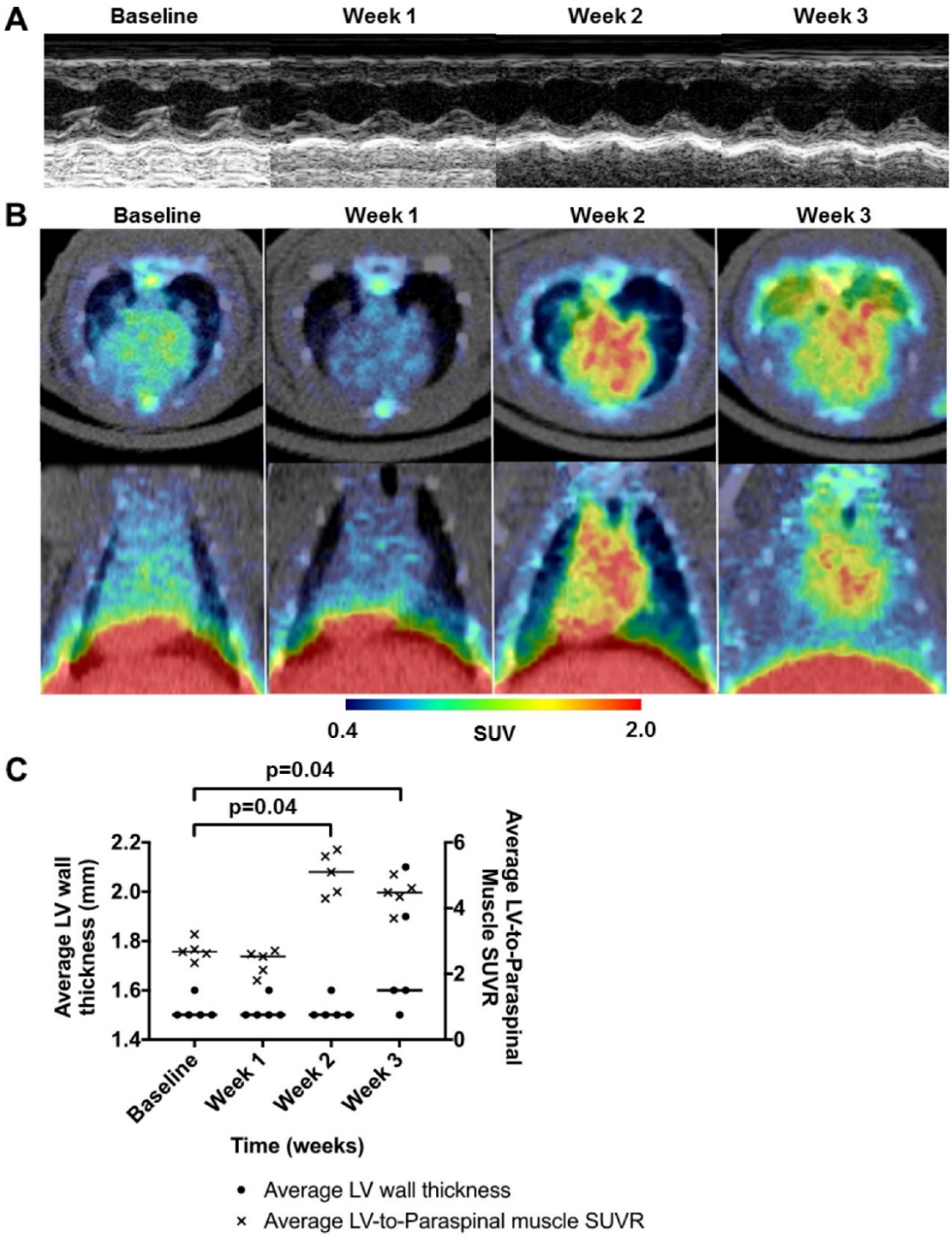

Figure 8. Utility of ^{68}Ga-NOTA-MSA PET for early detection of myocardial inflammation in myocarditis before structural changes in the myocardium. (A) Representative 2-dimensional echocardiography images of the left ventricular (LV) short-axis view at baseline, week 1, 2 and 3 after initiation of immunization. There was no difference in the LV wall thickness during this period. (B) Representative ^{68}Ga-NOTA-MSA PET images of the same rat in Figure 8A at baseline, week 1, 2 and 3 post-immunization. (C) Quantification of the ^{68}Ga-NOTA-MSA on PET and LV wall thickness on echocardiography. Significant rise of the ^{68}Ga-NOTA-MSA uptake is seen at week 2 on PET whereas the LV wall thickens at week 3 on echocardiography. The median value of each groups are shown as horizontal lines. SUV(R), standardized uptake value (ratio).

Contrary to the dose-dependent decrease of MSA uptake in macrophage cell line in vitro, the pattern of tracer uptake was upregulated in the heart and downregulated in the reticuloendothelial system in animals injected with unlabeled precursor (Figure 5). This kind of phenomenon has been used therapeutically in treating lymphoma patients with ibritumomab (Zevalin®), anti-CD20 antibody, where pretreatment with cold, unlabeled antibody is considered to enhance the binding of the labeled antibody to the cancer cells (29). Administration of the cold anti-CD20 antibody prior to the therapeutic antibodies emitting beta-radiation has shown to effectively block the vast reservoir of the antigens in

the bone marrow and spleen and therefore enhance the uptake of therapeutic antibodies to the lymphoma cells. Our results with the unlabeled MSA blockade are in agreement with these findings. Excess unlabeled MSA primarily blocked the labeled MSA uptake in major organs that serve as major reservoirs of inflammatory cells and prolonged the blood circulation of the labeled MSA. This may enhance the passive accumulation of the tracer in the myocardium and other organs (30,31). Furthermore, successful in vivo blockade of ^{68}Ga-NOTA-MSA uptake to the macrophages in the myocardium could be supported by the autoradiography result after administration of excess unlabeled MSA, which showed diffusely increased uptake in the myocardium.

Patients with myocarditis may not initially present with evidence of myocardial inflammation/edema and therefore, the diagnosis of myocarditis at an early stage of inflammation is clinically challenging (32). Although investigators have added the use of T2 magnetic resonance imaging for detection of myocardial edema (33), some have disputed its scientific basis (34). In a previous report using rat myocarditis model, abnormal magnetic resonance findings were not definite at 2 weeks after induction of myocarditis (35). In this respect, our findings showing clear ^{68}Ga-NOTA-MSA uptake at 2 weeks on PET after induction of myocarditis, which was earlier than myocardial edema on echocardiography, hold great promise for early diagnosis of these kinds of patients in doubt of diagnosis. Although earlier trials have failed to prove the efficacy of various immunosuppressive agents for myocarditis (36,37), this may be because myocarditis was diagnosed at a timepoint of 'no-return' (38,39). Additionally, the clear trend in the decrease of ^{68}Ga-NOTA-MSA uptake according to the duration of cyclosporine-A treatment suggests that ^{68}Ga-NOTA-MSA may be an effective tracer for monitoring the effect of treatment.

There are some limitations of our study/tracer. First, our study does not prove whether ^{68}Ga-NOTA-MSA is specific to imaging myocarditis or whether it targets various diseases associated with MR-positive macrophage infiltration. We think it would be the latter based on the findings that ^{68}Ga-NOTA-MSA can be used for tracking the sentinel lymph node (7,16) and also imaging atherosclerosis (40). It would be clinically interesting to expand our findings to other cardiovascular diseases as the importance of MR-positive macrophages is highlighted in various previous papers. Second, our data does not show directly that the MR is the receptor of ^{68}Ga-NOTA-MSA. However, albeit not the receptor of MSA, the pattern of colocalization of MR and MSA in the tissue sections suggests that MR is certainly a nodal mediator of MSA uptake in macrophages.

In conclusion, we have shown that ^{68}Ga-NOTA-MSA is unique in showing the degree of myocardial inflammation in myocarditis. More specifically, the results of our study demonstrate the potential utility of visualizing MR-positive macrophages, using ^{68}Ga-NOTA-MSA, in the diagnosis of myocarditis as well as in the follow-up of the efficacy of treatment or the disease course. Further studies in myocarditis patients, who suffer from the potentially fatal course of the disease, are warranted in the future for further expansion of this novel method.

Supplementary Material

Additional File 1:
Supplementary Figures.
http://www.thno.org/v07p0413s1.pdf
Additional File 2:
Movie S1. http://www.thno.org/v07p0413s2.avi
Additional File 3:
Movie S2. http://www.thno.org/v07p0413s3.avi

Abbreviations

2-(p-isothiocyanatobenzyl)-1,4,7-triazacyclononane-1,4,7-triacetic acid, NOTA; mannosylated human serum albumin, MSA; positron emission tomography, PET; human serum albumin, HSA; left ventricular, LV; end-diastolic/systolic dimensions, EDD/ESD; region of interest, ROI; standardized uptake value (ratio), SUV(R); rhodamine isothiocyanate, RITC; mannose receptor, MR; ^{18}F-fluorodeoxyglucose, ^{18}F-FDG.

Acknowledgements

We thank Mi-Kyung Hong, RDCS for the echocardiography, Mi Kyeong Hong, MS for the synthesis of the ^{68}Ga-NOTA-MSA and Young-Joo Kim for his help in the biodistribution assay. This study was supported by grants from the Korean Health Technology R&D Project (HI13C1961, HI15C0399, HI15C3093), Ministry of Health, Welfare & Family Affairs and the Basic Science Research Program through the National Research Foundation of Korea (2014R1A1A1003004), Ministry of Education, South Korea.

Competing Interests

The authors have declared that no competing interest exists.

References

1. Afanasyeva M, Georgakopoulos D, Belardi DF et al. Quantitative analysis of myocardial inflammation by flow cytometry in murine autoimmune myocarditis: correlation with cardiac function. *Am J Pathol* 2004;164:807-815.
2. Sagar S, Liu PP, Cooper LT, Jr. Myocarditis. *Lancet* 2012;379:738-747.
3. Cooper LT, Baughman KL, Feldman AM et al. The role of endomyocardial biopsy in the management of cardiovascular disease: a scientific statement from the American Heart Association, the American College of Cardiology, and the European Society of Cardiology. Endorsed by the Heart Failure Society of America and the Heart Failure Association of the European Society of Cardiology. *J Am Coll Cardiol* 2007;50:1914-1931.
4. Smith SC, Ladenson JH, Mason JW, Jaffe AS. Elevations of cardiac troponin I associated with myocarditis. Experimental and clinical correlates. *Circulation* 1997;95:163-168.
5. Skouri HN, Dec GW, Friedrich MG, Cooper LT. Noninvasive imaging in myocarditis. *J Am Coll Cardiol* 2006;48:2085-2093.
6. Leuschner F, Courties G, Dutta P et al. Silencing of CCR2 in myocarditis. *Eur Heart J* 2015;36:1478-1488.
7. Choi JY, Jeong JM, Yoo BC et al. Development of 68Ga-labeled mannosylated human serum albumin (MSA) as a lymph node imaging agent for positron emission tomography. *Nucl Med Biol* 2011;38:371-379.
8. Ishiyama S, Hiroe M, Nishikawa T et al. The Fas/Fas ligand system is involved in the pathogenesis of autoimmune myocarditis in rats. *J Immunol* 1998;161:4695-4701.
9. Moon H, Park HE, Kang J et al. Noninvasive assessment of myocardial inflammation by cardiovascular magnetic resonance in a rat model of experimental autoimmune myocarditis. *Circulation* 2012;125:2603-2612.
10. Choi H, Kim YK, Kang H et al. Abnormal metabolic connectivity in the pilocarpine-induced epilepsy rat model: a multiscale network analysis based on persistent homology. *Neuroimage* 2014;99:226-236.
11. Eo JS, Paeng JC, Lee S et al. Angiogenesis imaging in myocardial infarction using 68Ga-NOTA-RGD PET: characterization and application to therapeutic efficacy monitoring in rats. *Coron Artery Dis* 2013;24:303-311.
12. McEnery MW, Snowman AM, Trifiletti RR, Snyder SH. Isolation of the mitochondrial benzodiazepine receptor: association with the voltage-dependent anion channel and the adenine nucleotide carrier. *Proc Natl Acad Sci U S A* 1992;89:3170-3174.
13. Morin D, Musman J, Pons S, Berdeaux A, Ghaleb B. Mitochondrial translocator protein (TSPO): From physiology to cardioprotection. *Biochem Pharmacol* 2016;105:1-13.
14. Zhang S, Kodama M, Hanawa H, Izumi T, Shibata A, Masani F. Effects of cyclosporine, prednisolone and aspirin on rat autoimmune giant cell myocarditis. *J Am Coll Cardiol* 1993;21:1254-1260.
15. Haroon A, Zumla A, Bomanji J. Role of fluorine 18 fluorodeoxyglucose positron emission tomography-computed tomography in focal and generalized infectious and inflammatory disorders. *Clin Infect Dis* 2012;54:1333-1341.
16. Jeong JM, Hong MK, Kim YJ et al. Development of 99mTc-neomannosyl human serum albumin (99mTc-MSA) as a novel receptor binding agent for sentinel lymph node imaging. *Nucl Med Commun* 2004;25:1211-1217.
17. Kim HK, Kim S, Park JJ, Jeong JM, Mok YJ, Choi YH. Sentinel node identification using technetium-99m neomannosyl human serum albumin in esophageal cancer. *Ann Thorac Surg* 2011;91:1517-1522.
18. Fujiu K, Wang J, Nagai R. Cardioprotective function of cardiac macrophages. *Cardiovasc Res* 2014;102:232-239.
19. Cihakova D, Barin JG, Afanasyeva M et al. Interleukin-13 protects against experimental autoimmune myocarditis by regulating macrophage differentiation. *Am J Pathol* 2008;172:1195-1208.
20. Fairweather D, Cihakova D. Alternatively activated macrophages in infection and autoimmunity. *J Autoimmun* 2009;33:222-230.
21. James OG, Christensen JD, Wong TZ, Borges-Neto S, Koweek LM. Utility of FDG PET/CT in inflammatory cardiovascular disease. *Radiographics* 2011;31:1271-1286.
22. Takano H, Nakagawa K, Ishio N et al. Active myocarditis in a patient with chronic active Epstein-Barr virus infection. *Int J Cardiol* 2008;130:e11-13.
23. Nensa F, Kloth J, Tezgah E et al. Feasibility of FDG-PET in myocarditis: Comparison to CMR using integrated PET/MRI. *J Nucl Cardiol* 2016.
24. Tahara N, Mukherjee J, de Haas HJ et al. 2-deoxy-2-[18F]fluoro-D-mannose positron emission tomography imaging in atherosclerosis. *Nat Med* 2014;20:215-219.
25. Hackstein H, Taner T, Logar AJ, Thomson AW. Rapamycin inhibits macropinocytosis and mannose receptor-mediated endocytosis by bone marrow-derived dendritic cells. *Blood* 2002;100:1084-1087.
26. Nahrendorf M, Zhang H, Hembrador S et al. Nanoparticle PET-CT imaging of macrophages in inflammatory atherosclerosis. *Circulation* 2008;117:379-387.
27. Niu G, Lang L, Kiesewetter DO et al. In Vivo Labeling of Serum Albumin for PET. *J Nucl Med* 2014;55:1150-1156.
28. Chang YS, Jeong JM, Lee YS et al. Preparation of 18F-human serum albumin: a simple and efficient protein labeling method with 18F using a hydrazone-formation method. *Bioconjug Chem* 2005;16:1329-1333.
29. Dillman RO. Radiolabeled anti-CD20 monoclonal antibodies for the treatment of B-cell lymphoma. *J Clin Oncol* 2002;20:3545-3557.
30. Im HJ, England CG, Feng L et al. Accelerated Blood Clearance Phenomenon Reduces the Passive Targeting of PEGylated Nanoparticles in Peripheral Arterial Disease. *ACS Appl Mater Interfaces* 2016;8:17955-17963.
31. England CG, Im HJ, Feng L et al. Re-assessing the enhanced permeability and retention effect in peripheral arterial disease using radiolabeled long circulating nanoparticles. *Biomaterials* 2016;100:101-109.
32. Dennert R, Crijns HJ, Heymans S. Acute viral myocarditis. *Eur Heart J* 2008;29:2073-2082.
33. Friedrich MG, Sechtem U, Schulz-Menger J et al. Cardiovascular magnetic resonance in myocarditis: A JACC White Paper. *J Am Coll Cardiol* 2009;53:1475-1487.
34. Kim HW, Van Assche L, Jennings RB et al. Relationship of T2-Weighted MRI Myocardial Hyperintensity and the Ischemic Area-At-Risk. *Circ Res* 2015;117:254-265.
35. Rinkevich-Shop S, Konen E, Kushnir T et al. Non-invasive assessment of experimental autoimmune myocarditis in rats using a 3 T clinical MRI scanner. *Eur Heart J Cardiovasc Imaging* 2013;14:1069-1079.
36. Mason JW, O'Connell JB, Herskowitz A et al. A clinical trial of immunosuppressive therapy for myocarditis. The Myocarditis Treatment Trial Investigators. *N Engl J Med* 1995;333:269-275.
37. McNamara DM, Holubkov R, Starling RC et al. Controlled trial of intravenous immune globulin in recent-onset dilated cardiomyopathy. *Circulation* 2001;103:2254-2259.
38. Wojnicz R, Nowalany-Kozielska E, Wojciechowska C et al. Randomized, placebo-controlled study for immunosuppressive treatment of inflammatory dilated cardiomyopathy: two-year follow-up results. *Circulation* 2001;104:39-45.
39. Frustaci A, Chimenti C, Calabrese F, Pieroni M, Thiene G, Maseri A. Immunosuppressive therapy for active lymphocytic myocarditis: virological and immunologic profile of responders versus nonresponders. *Circulation* 2003;107:857-863.
40. Kim EJ, Kim S, Seo HS et al. Novel PET Imaging of Atherosclerosis with 68Ga-Labeled NOTA-Neomannosylated Human Serum Albumin. *J Nucl Med* 2016;57:1792-1797.